17th World Conference on Earthquake Engineering, 17WCEE
Sendai, Japan - September 13th to 18th 2020

A Generalized Model of Approximated Rate-independent Linear Damping Incorporated into Base-isolated Structures

H. Luo[(1)], K. Ikago[(2)]

[(1)] *PhD student, School of Engineering, Tohoku University, luo.hao.q1@dc.tohoku.ac.jp*
[(2)] *Professor, International Research Institute of Disaster Science, Tohoku University, ikago@irides.tohoku.ac.jp*

Abstract

During the 2011 Great East Japan Earthquake, some base-isolated structures that were perceived to be safe, suffered damages in lead dampers due to large isolator deformations. For suppressing these excessive deformations, the number of installed dampers (e.g., oil dampers or metal yielding dampers) in the isolation layer could be increased, therefore supplementing more damping. However, it may result in an increased floor response acceleration and may consequently compromises the effect of base isolation. Rate-independent linear damping (RILD) is considered to be a promising solution to this problem as it can benefit a low-frequency structure subjected to extreme earthquake events by reducing response displacement without increasing floor response acceleration. It is established that an ideal RILD, having a dynamic stiffness whose real and imaginary parts are both independent of vibration frequency, cannot be physically realized due to its non-causality, which might hinder its practical applications. In the past decades, several causal models (e.g., Biot, Makris, and Keivan models) were proposed for approximating the ideal non-causal RILD. However, past studies primarily focused on the applications of RILD into linear structural systems; thus, the studies on causal approximations of RILD, which apply to nonlinear structural systems, are still limited.

In this study, a generalized model is proposed for the causal approximation of RILD using fractional derivatives, and its application in the isolation layer of a base-isolated building structure to constraint the isolator deformation is discussed. The proposed model is characterized by a tuning parameter varying between zero and unity. An interesting finding to note is that, in the limiting cases of tuning parameter equal to zero and unity, the proposed model reduces to Makris and Keivan models, respectively. It means that the proposed model represents a continuous transformation from Makris to Keivan models with the tuning parameter increasing from zero to unity, i.e., it is indeed a generalized model of causally approximated RILD. Moreover, an alternative physical representation of the proposed model is constructed by arranging a linear spring, a linear negative stiffness element, and a fractional-order Maxwell element coupled with each other in parallel. For the numerical implementation of the proposed model, a time-domain analysis technique is developed, which can be incorporated into established numerical integration schemes, enabling time-history dynamic analyses of a structural system incorporated with the proposed model to be readily conducted. For illustrating the effectiveness of the developed technique for nonlinear dynamic analyses, a five-story base-isolated building structure is used as an analytical example, and a hysteretic damper and the proposed RILD element are simultaneously incorporated into the isolation layer for providing additional damping in order to constraint the isolator displacements. Several nonlinear dynamic analyses verify the effectiveness of the developed time-domain technique. Furthermore, parametric studies are conducted to investigate the effect of the tuning parameter on the seismic performance of the controlled structure.

Keywords: Rate-independent linear damping; fractional derivative; nonlinear dynamic analysis; base-isolation.

1. Introduction

During the 2011 Great East Japan Earthquake, some base-isolated building structures, which were considered to be safe, suffered damages in lead dampers due to large isolator deformations. It poses a grave concern for the seismically isolated structures, which might suffer excessive displacements beyond the design limit in the events of an extreme earthquake, such as the future expected Nankai mega-thrust earthquake in Japan and the Cascadia earthquake in North America. Indeed, larger number of traditional damping devices (e.g., oil dampers or metal yielding dampers) may be installed in the isolation layer so that higher damping can be supplemented to suppress these excessive deformations. However, it may result in an increased floor response acceleration and consequently compromises the effect of base isolation.

Rate-independent linear damping (RILD) is considered to be a promising solution for achieving an effective reduction in the response displacement of a low-frequency structure without the increasing floor response acceleration [1]. However, due to its non-causality, RILD cannot be physically realized [2], and the primary challenge is to find a causal method to approximate it so that physical damping devices can be developed for its practical applications. In the past decades, various causal models were proposed to approximate RILD, e.g., Biot model [3, 4] and Makris model [5]. As pointed out by Makris [5], the latter is actually a high-frequency limiting case of the former. Recently, a first-order all-pass filter was used by Keivan et al. [6, 7] as a simple causal approximation of RILD. Such a filter can be passively realized using a mechanical system consisting of a negative stiffness element and a Maxwell element coupled in parallel [8, 9]. Further investigation shows that this filter is mathematically related to the Biot model by Mercator series, and can be used as a first-order approximation of the latter [10]. However, these past studies primarily focused on the applications of RILD into linear structures; thus, the studies on causal approximations of RILD, which apply to nonlinear structural systems, are still limited. In this study, a generalized model is proposed for the causal approximation of RILD using fractional derivatives, and its application in the isolation layer of a base-isolated building structure for providing supplemental damping to constraint the isolator deformation is discussed.

2. Rate-independent linear damping

2.1 Existing models for RILD

A popular model for RILD, known as complex stiffness, consists of a linear spring element and an ideal RILD element coupled in parallel, and is usually expressed in terms of the dynamic stiffness as follows:

$$\mathcal{H}_{\mathrm{I}}(i\omega) = k_0\left[1 + \eta Z_{\mathrm{I}}(i\omega)\right] \tag{1}$$

where k_0 is the spring stiffness; $i = \sqrt{-1}$; η denotes the loss factor; $Z(i\omega)$ is the normalized dynamic stiffness of an ideal RILD element, also known as the unit imaginary function described as follows

$$Z_{\mathrm{I}}(i\omega) = i\ \mathrm{sgn}(\omega) \tag{2}$$

where $\mathrm{sgn}(\cdot)$ denotes the signum function. However, due to its non-causality, this model cannot be physically realized [2], but may be approximated by using causal methods for its practical applications. Till this end, various models have been proposed, as listed in Table 1. For example, Keivan et al. [6] used a first-order all-pass filter to approximate the RILD, defined as follows:

$$Z_{\mathrm{K}}(i\omega) = \frac{i\omega - \varepsilon}{i\omega + \varepsilon} \tag{3}$$

which can provide an amplitude of unity all over the frequencies, as does Eq.(2), and a phase advanced to the deformation by $\pi/2$ rad at $\omega = \varepsilon$. This filter can be realized by either a semi-active method [6, 7] or a passive method [8], and can be used as a viable option to mimic the ideal RILD for seismic protection of low-frequency structures [9].

Table 1 – Different models for RILD

Model	**Dynamic stiffness**	**Causality**
Ideal RILD	$k_0[1+i\ \eta\ \mathrm{sgn}(\omega)]$	Non-causal
Biot [3, 4]	$k_0\left\{1+\dfrac{\eta}{\pi}\ln\left[1+\left(\dfrac{\omega}{\varepsilon}\right)^2\right]+i\ \dfrac{2\eta}{\pi}\mathrm{atan}\left(\dfrac{\omega}{\varepsilon}\right)\right\}$	Causal
Makris [5]	$k_0\left[1+\dfrac{2\eta}{\pi}\ln\left\lvert\dfrac{\omega}{\varepsilon}\right\rvert+i\ \eta\ \mathrm{sgn}\left(\dfrac{\omega}{\varepsilon}\right)\right]$	Causal
Keivan et al. [6]	$k_0\left(1+\eta\dfrac{i\omega-\varepsilon}{i\omega+\varepsilon}\right)$	Causal
The proposed	$k_0\left[1+\eta\ \cot\left(\dfrac{\alpha\pi}{4}\right)\dfrac{(i\omega)^\alpha-\varepsilon^\alpha}{(i\omega)^\alpha+\varepsilon^\alpha}\right]$	Causal

2.2 The proposed model

In this study, the first-order causal filter expressed in Eq. (3) is further extended and generalized into a fractional-order filter defined as follows:

$$Z_{\mathrm{P}}(i\omega)=\beta_\alpha\frac{(i\omega)^\alpha-\varepsilon^\alpha}{(i\omega)^\alpha+\varepsilon^\alpha} \tag{4}$$

where α is a real-valued tuning parameter $(0\le\alpha\le1)$; $\beta_\alpha=\cot(\alpha\pi/4)$ is an adjusting factor for unity amplitude at $\omega=\varepsilon$; $(i\omega)^\alpha$ is uniquely defined as $(i\omega)^\alpha=|\omega|^\alpha\mathrm{Exp}[i\ \mathrm{sgn}(\omega)\alpha\pi/2]$. Obviously, with $\alpha=1$, the above filter reduces to Eq.(3). However, when compared to a first-order all-pass filter, the proposed filter with a smaller tuning parameter (e.g., $\alpha=0.1$) has a less rate-dependent imaginary part. It thus provides an improved approximation of an ideal RILD element in terms of the loss modulus, as shown in Fig. 1(b).

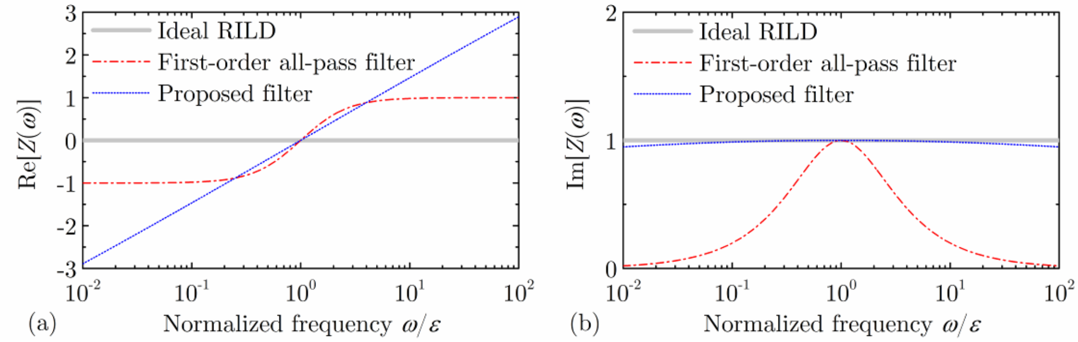

Fig. 1 – Comparison between approximated and ideal RILD elements: (a) storage and (b) loss moduli

Corresponding to Eq.(1), a fractional-order model of approximated RILD is proposed by using the generalized filter, and its dynamic stiffness is expressed as follows

$$\mathcal{H}_{\mathrm{P}}(i\omega)=k_0\left[1+\eta\beta_\alpha\frac{(i\omega)^\alpha-\varepsilon^\alpha}{(i\omega)^\alpha+\varepsilon^\alpha}\right] \tag{5}$$

The causality of this model has been confirmed [11], and thus it may be realized by the use of physical systems. To this end, an alternative mechanical system is constructed to represent the proposed model, as shown in Fig. 2(a). For comparison, Fig. 2(b) depicts a Maxwell-Wiechert model, which can be used to represent the Biot model [4].

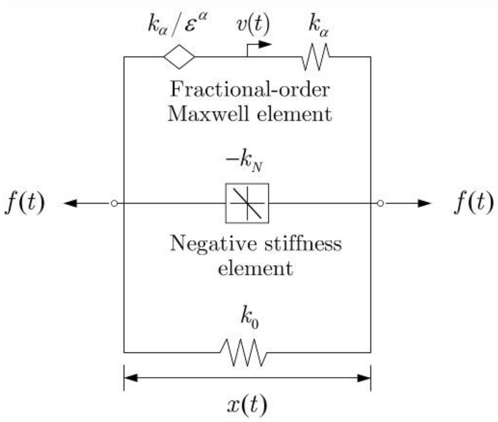

(a) The proposed model

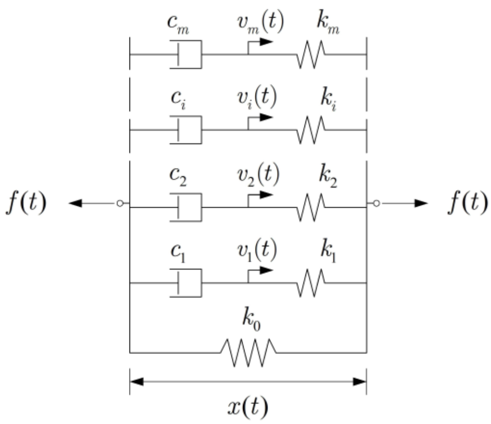

(b) A Maxwell-Wiechert model

Fig. 2 – Mechanical representations of approximated models for approximation of RILD

For the mechanical system shown in Fig. 2(a), a fractional-order Maxwell element [12, 13] is coupled in parallel with a linear spring and a negative stiffness element [14, 15]. Furthermore, it has to be proved that this mechanical system can be used to represent the proposed model. The fractional-order Maxwell element is represented by a linear spring in series with a fractional-order dashpot. The equation of motion of such a fractional-order element can be expressed as follows

$$D_{0+}^{\alpha}v(t) + \varepsilon^{\alpha}v(t) = \varepsilon^{\alpha}x(t) \tag{6}$$

where $D_{0+}^{\alpha}v(t)$ denotes an α-order derivative of $v(t)$ with respect to time t. Here, the Riemann-Liouville's definition [16] of the fractional derivative is used and is defined as follows

$$D_{0+}^{\alpha}v(t) = \frac{1}{\Gamma(1-\alpha)}\frac{d}{dt}\int_0^t \frac{v(\tau)}{(t-\tau)^{\alpha}}d\tau \tag{7}$$

where $\Gamma(\cdot)$ is the Euler's Gamma function. By using the property of fractional derivative [16], one has

$$\mathcal{F}[D_{0+}^{\alpha}v(t)] = (i\omega)^{\alpha}\mathcal{F}[v(t)] = (i\omega)^{\alpha}V(i\omega) \tag{8}$$

where $\mathcal{F}(\cdot)$ denotes the Fourier transform. Thus, applying Fourier transform to Eq. (6) gives

$$V(i\omega) = \frac{\varepsilon^{\alpha}}{(i\omega)^{\alpha} + \varepsilon^{\alpha}}X(i\omega) \tag{9}$$

The total response force provided by this mechanical system is written in the frequency domain as follows:

$$F(i\omega) = (k_0 - k_N)X(i\omega) + k_\alpha[X(i\omega) - V(i\omega)] \tag{10}$$

With $k_N = \eta\beta_\alpha k_0$ and $k_\alpha = 2\eta\beta_\alpha k_0$, substituting Eq.(9) into Eq.(10) gives its dynamic stiffness as follows:

$$\mathcal{H}(i\omega) = k_0\left[1 + \eta\beta_\alpha\frac{(i\omega)^{\alpha} - \varepsilon^{\alpha}}{(i\omega)^{\alpha} + \varepsilon^{\alpha}}\right] \tag{11}$$

which coincides with the dynamic stiffness of the proposed model expressed in Eq.(5). This verifies that the proposed model can be physically represented by such a mechanical system.

2.3 Relationship between Makris and the proposed models

Here, it is to be shown that the proposed model can include Makris model as a special case of $\alpha = 0$. Initially, the case of $\omega > 0$ is considered. Letting $(i\omega)^\alpha = \omega^\alpha[\cos(\alpha\pi/2) + i\sin(\alpha\pi/2)]$ and $\lambda = \omega/\varepsilon$, the real and imaginary parts of Eq.(4) can be obtained as follows, respectively,

$$\mathcal{Re}[Z_P(i\lambda)] = \cot\left(\frac{\alpha\pi}{4}\right)\frac{\lambda^{2\alpha}-1}{1+\lambda^{2\alpha}+2\lambda^\alpha\cos(\alpha\pi/2)} \tag{12}$$

$$\mathcal{Im}[Z_P(i\lambda)] = \cot\left(\frac{\alpha\pi}{4}\right)\frac{2\lambda^\alpha\sin(\alpha\pi/2)}{1+\lambda^{2\alpha}+2\lambda^\alpha\cos(\alpha\pi/2)} \tag{13}$$

Let $y = \lambda^{2\alpha}$, then $\alpha = \ln y/(2\ln\lambda)$, therefore

$$\lim_{\alpha\to 0}\mathcal{Re}[Z_P(i\lambda)] = \lim_{\alpha\to 0}\frac{\lambda^{2\alpha}-1}{4\tan(\alpha\pi/4)} = \lim_{\alpha\to 0}\frac{\lambda^{2\alpha}-1}{\alpha\pi} = \frac{2}{\pi}\ln\lambda\ \lim_{y\to 1}\frac{y-1}{\ln y} = \frac{2}{\pi}\ln\lambda \tag{14}$$

With respect to the imaginary part, we have

$$\lim_{\alpha\to 0}\mathcal{Im}[Z_P(i\lambda)] = \lim_{\alpha\to 0}\frac{2\lambda^\alpha\sin(\alpha\pi/2)}{4\tan(\alpha\pi/4)} = 1 \tag{15}$$

Thus, recall that $\lambda = \omega/\varepsilon$, as $\alpha \to 0$, we can obtain

$$Z_P(i\omega) = \mathcal{Re}[Z_P(i\omega)] + i\,\mathcal{Im}[Z_P(i\omega)] = \frac{2}{\pi}\ln\left(\frac{\omega}{\varepsilon}\right) + i\,,\ \ \omega > 0. \tag{16}$$

For $\omega < 0$, changing the valuable ω to $-\omega$ and following the above procedures, as $\alpha \to 0$, we can obtain

$$Z_P(i\omega) = \frac{2}{\pi}\ln\left(-\frac{\omega}{\varepsilon}\right) - i\,,\ \ \omega < 0. \tag{17}$$

Summarizing Eqs. (16) and (17) yields

$$Z_P(i\omega) = \frac{2}{\pi}\ln\left|\frac{\omega}{\varepsilon}\right| + i\ \mathrm{sgn}\left(\frac{\omega}{\varepsilon}\right) \tag{18}$$

Thus, as $\alpha \to 0$, the dynamic stiffness of the proposed model reduces to

$$\mathcal{H}_P(i\omega) = k_0[1+\eta Z_P(i\omega)] = k_0\left[1+\frac{2}{\pi}\eta\ln\left|\frac{\omega}{\varepsilon}\right| + i\ \eta\,\mathrm{sgn}\left(\frac{\omega}{\varepsilon}\right)\right] \tag{19}$$

which coincides with that of the Makris model, as shown in Table 1. Recall that the proposed model reduces to the Keivan model when $\alpha = 1$, therefore, the proposed model actually represents a continuous transformation from the Makris model to the Keivan model with the increase in the tuning parameter α from zero to unity, i.e., it is indeed a generalized model of causally approximated RILD. Since the dynamic stiffness of the proposed model continuously varies with the tuning parameter α, it can be predicted that the proposed model with a small tuning parameter (e.g., $\alpha = 0.1$) can provide a good approximation of the Makris model over a frequency range of interest.

For example, setting $\eta = 0.1$, Fig. 3 compares the normalized dynamic stiffness of the proposed model (e.g., $\alpha = 0.1$) with that of the Makris and the Biot models. It is shown in Fig. 3 that the differences between the dynamic stiffness of the proposed model with $\alpha = 0.1$ and that of the Makris model are negligible over the frequency range of interest. This indicates that the proposed model with a small tuning parameter α can be used to approximate the Makris model without significant loss of accuracy. Because of the relationship between the Biot and the Makris models, i.e., the latter is actually a high-frequency limiting case of the former, the proposed model with a small tuning parameter (e.g., $\alpha = 0.1$) can also be used to approximate the high-frequency characteristics of the Biot model, as shown in Fig. 3.

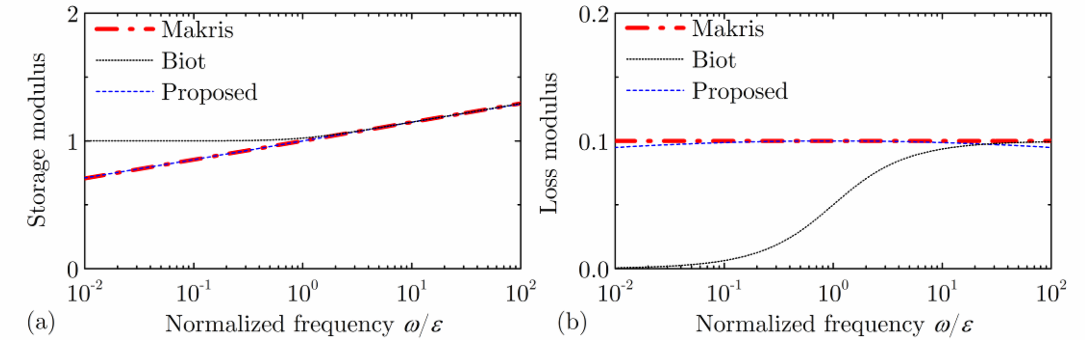

Fig. 3 – Comparison between the different approximated RILD models: (a) storage and (b) loss moduli

3. Numerical implementation of the proposed model

Here, we consider a linear single-degree-of-freedom (SDOF) system incorporated with the proposed model, as shown in Fig. 4, whose governing equations of motion are expressed as follows

$$\begin{cases} m\ddot{x}(t) + (k_0 + k_\alpha - k_N)x(t) - k_\alpha v(t) = p(t) \\ D_{0+}^{\alpha}v(t) + \varepsilon^{\alpha}v(t) = \varepsilon^{\alpha}x(t) \end{cases} \tag{20}$$

For the above system, frequency-domain methods using fast Fourier transform (FFT) algorithm can be applied to carry out dynamic analyses. However, time-domain methods may be preferred in some cases, e.g., where nonlinear behaviors of the structural and/or supplemental energy dissipation elements are involved.

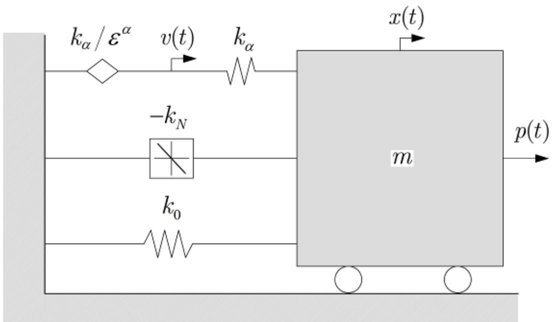

Fig. 4 – An SDOF system incorporated with the proposed model

A time-domain technique for dynamic analysis of the above system is developed on the basis of the so-called L1-algorithm [16], which can be used to evaluate the Reimann-Liouville's type of fractional derivative. To this end, the definition given in Eq. (7) is equivalently expressed as follows:

$$D_{0+}^{\alpha}v(t) = \frac{1}{\Gamma(1-\alpha)}\left[\frac{v(0)}{t^{\alpha}} + \int_0^t \frac{1}{\tau^{\alpha}}\frac{dv(t-\tau)}{d\tau}d\tau\right] \tag{21}$$

Letting the time axis be divided into N subintervals of an equal length $h = t/n$ and $t = t_n = nh$ $(1 \le n \le N)$, the above equation can be approximated as follows:

$$D_{0+}^{\alpha}v(t_n) \approx \frac{1}{\Gamma(2-\alpha)h^{\alpha}}\sum_{j=0}^{n} L_j v(t_{n-j}) \tag{22}$$

where L_j is a weighting factor independent of the function $v(t)$, with $L_0 = 1$ and

$$L_j = \begin{cases} (j+1)^{1-\alpha} - 2j^{1-\alpha} + (j-1)^{1-\alpha}, & j = 1,2,\dots,n-1; \\ (1-\alpha)j^{-\alpha} - j^{1-\alpha} + (j-1)^{1-\alpha}, & j = n. \end{cases}$$

Recall that $k_N = \eta\beta_\alpha k_0$ and $k_\alpha = 2\eta\beta_\alpha k_0$, let $x(t_n) = x(t)$, and then substituting Eq. (22) into the second equation in Eq.(20) gives the relationship between $v(t_n)$ and $x(t_n)$ as follows:

$$v(t_n) = \frac{\psi}{1+\psi}x(t_n) - \frac{1}{1+\psi}Q(t_{n-1}) \tag{23}$$

where $\psi = \varepsilon^\alpha h^\alpha \Gamma(2-\alpha)$ and $Q(t_{n-1}) = \sum_{j=1}^{n} L_j v(t_{n-j})$. Substituting Eqs. (22) and (23) into Eq.(20) gives

$$m\ddot{x}(t_n) + k_0 x(t_n) + f_D(t_n) = p(t_n) \tag{24}$$

where $f_D(t_n)$ is the damping force provided by the proposed RILD element, which is expressed as follows:

$$f_D(t_n) = (k'_\alpha - k_N)x(t_n) + k'_\alpha Q(t_{n-1}) \tag{25}$$

where $k'_\alpha = k_\alpha/(1+\psi)$. Recall that the term $Q(t_{n-1})$ is only dependent on the past series $v(t_j)$, $j = 1,2,\dots,n-1$. Putting on the r.h.s. of Eq.(24), $k'_\alpha Q(t_{n-1})$ can be equivalently regarded as a fictitious force excitation. This makes the above system readily analyzed in a way similar to the case of an un-damped one.

The above time-domain analysis technique can be readily incorporated into established numerical integration schemes, e.g., the Newmark integration scheme, and thus, the time-history dynamic analyses can be conducted to investigate the dynamic behavior of the structural systems incorporated with the proposed model. It can also be readily extended to multi-degree-of-freedom structural systems for both linear and nonlinear dynamic analyses. When nonlinear behaviors of the structural and/or the supplemental energy dissipation elements are involved, the above time-domain technique can be readily applied using the Newton-Raphson's method for evaluating the behaviors of those nonlinear elements.

4. Numerical examples

In this study, a benchmark base-isolated five-story shear building model is used as an analytical example for time-history dynamic analyses, and Fig. 5 shows the structural specifications. The fundamental natural period and the inherent damping ratio of the first mode of the upper structure with a fixed base are approximately 0.67 s and 2%, respectively. The damping matrix of the upper structure is assumed to be proportional to the stiffness matrix. The natural rubber bearings are designed to have the isolation period as 4.0 s. However, the inherent damping of the isolators is neglected (i.e., $c_0 = 0$).

For providing supplemental damping to constraint the isolator displacement, a hysteretic damper (HD) and an RILD element are simultaneously incorporated into the isolation layer. In Fig. 5(b), the characteristic parameters of an HD are specified and μ denotes the ratio of yielding force to the total weight of the structural system (including the base weight $m_0 g$, where g denotes the gravitational acceleration). Besides its dissipation capability, an HD is used in base-isolated structures to provide sufficient initial stiffness to resist wind loads. Following the standard practice in Japan, the HD should be designed not to yield against the wind load of a 500-years return period. For satisfying this demand, the HD is designed with a yielding force of $4011\ \mathrm{kN}$, and the ratio of HD yielding force to the total weight is $\mu = 3.2\%$. It is established that due to its non-causality, an ideal RILD element is difficult to be used when a structural and/or supplemental energy dissipation element yields and exhibits strong nonlinear behavior. In such a case, the proposed causal RILD element, as shown in Fig. 5(c), may be used as a causal approximation of the ideal RILD element.

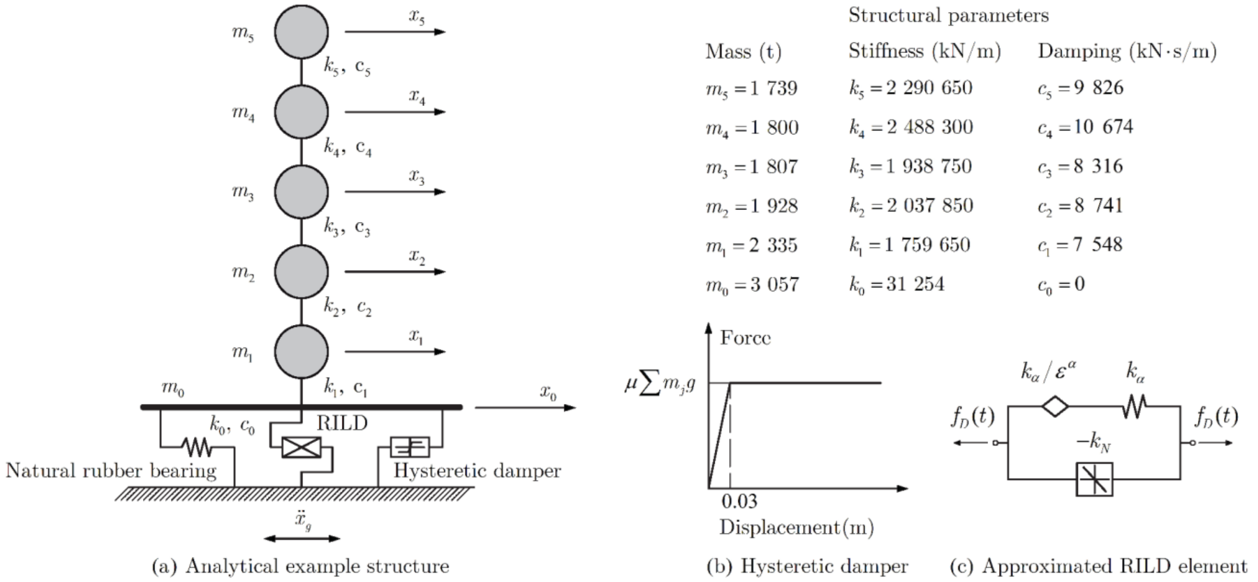

Fig. 5 – A base-isolated building structure incorporated with RILD

Time history analyses are conducted to investigate the seismic performance of a base-isolated structure incorporated with RILD by using three ground motion records and three types of synthetic ground motions as design earthquakes in accordance with the standard practice in Japan. The acceleration spectra of these ground motions are shown in Fig. 6. The three ground motion records are scaled so that their peak ground velocities (PGVs) are 0.5 m/s. The spectral accelerations of the synthetic ground motion are compatible with the target spectrum, which is also shown in Fig. 6(b). Amplification properties of a typical surface subsoil are considered for determining the target spectrum in accordance with the building design codes in Japan. The phase properties of the recorded ground motions as shown in Fig. 6(b) are used to synthesize the ground motion time-histories.

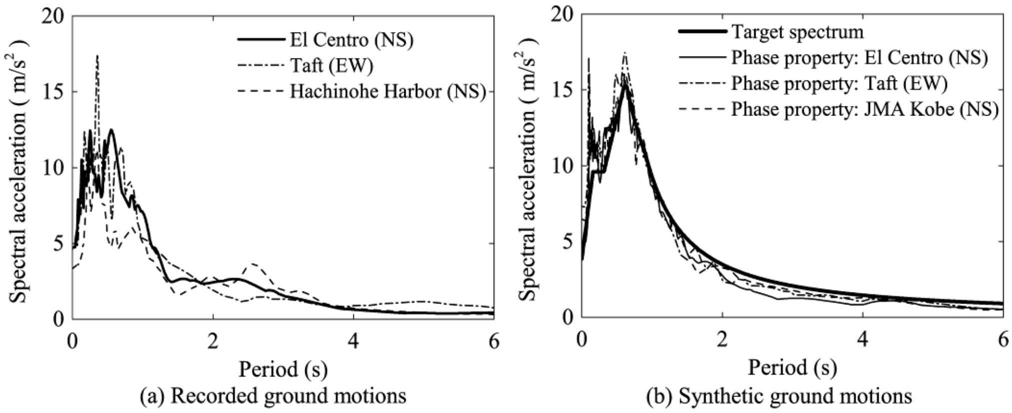

Fig. 6 – Acceration spetra [9]

4.1 Linear time-history analyses

In order to verify the accuracy of the proposed RILD element to causally approximate the ideal one, letting $\mu = 0$ (so that the structural system remains linearly elastic), the seismic performances of the base-isolated structure separately incorporated with ideal non-causal and the proposed RILD elements are compared by conducting time-history dynamic analyses. It should be mentioned that for the ideal RILD element, linear time-history analyses are carried out in the frequency-domain with the entire time history of input ground motion provided. For the proposed RILD element, the time-domain technique introduced in the above section is employed for dynamic analyses.

For example, letting $\eta = 0.4$, Fig. 7 compares the time-history responses of the example structure separately incorporated with different RILD elements. Here, two values of α are considered for the proposed RILD elements: (i) $\alpha = 1$ representing Keivan RILD element (first-order all-pass filter), (ii) $\alpha = 0.1$ approximating a Makris RILD element (excluding the linear stiffness element in the Makris model). It is shown that the differences between the seismic responses of the three systems are negligible. This occurs because the hysteresis loops of these RILD elements are similar, as shown in Fig. 8. This example verifies that both the Keivan and the Makris models can be used to approximate ideal RILD for application in a base-isolated structures without significant loss of accuracy.

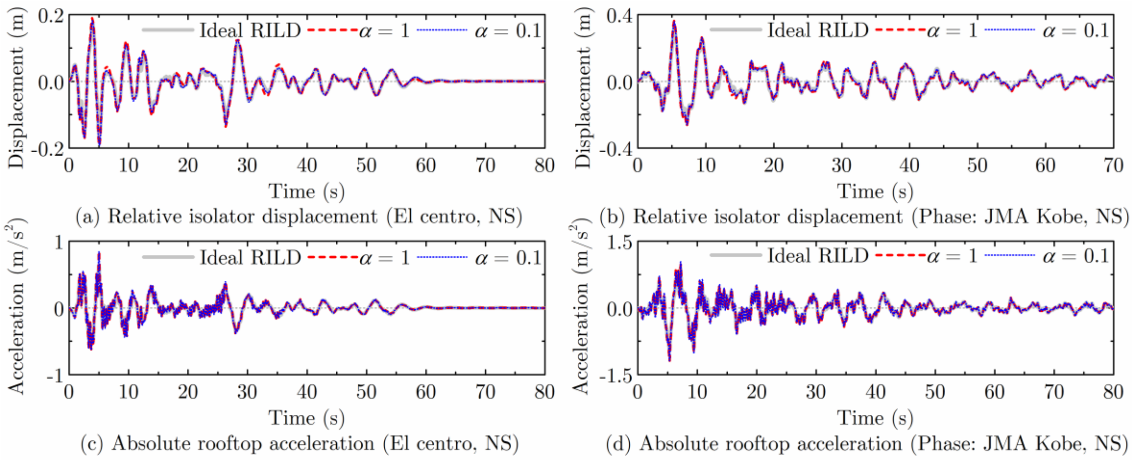

Fig. 7 – Time-history responses of a base-isolated structure incorporated with RILD (linear case)

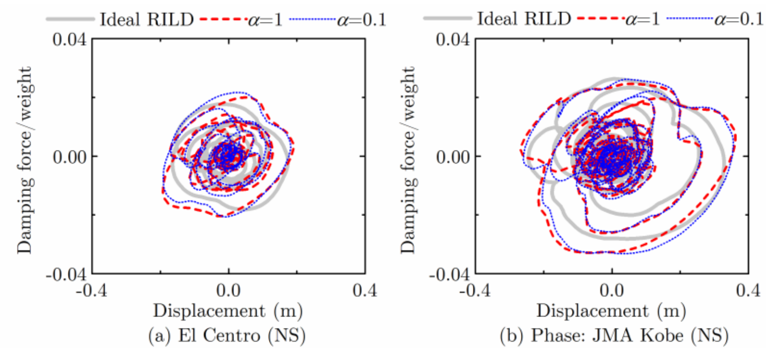

Fig. 8 – Hysteresis loops of different RILD elements

4.2 Nonlinear time-history analyses

Since the ideal non-causal RILD element is hard to be used for dynamic analyses in cases, where strong non-linearities of structural and/or supplemental energy dissipation elements are involved, it is necessary to use the approximated causal RILD elements instead. For verifying the capability of the proposed model used in such cases, nonlinear time-history analyses are conducted by employing the time-domain technique introduced in the above section.

For example, letting $\mu = 3.2\%$ and $\eta = 0.4$, Fig. 9 shows the time history responses of the example structure incorporated with the proposed RILD element. Also, two values of α are considered for the proposed RILD elements: $\alpha = 1$ and $\alpha = 0.1$, corresponding to the Keivan RILD element and an approximation of the Makris RILD element, respectively. It is shown that the differences between the seismic responses of the two systems are negligible. This is observed because the proposed RILD elements in these two cases behave similarly, as shown in Fig. 10, where hysteresis loops of HDs are also depicted. This example verifies that by using the time-domain technique introduced above, the proposed approximated RILD element can be used for nonlinear dynamic analyses, which are hard for an ideal non-causal RILD element. It should also be mentioned that for the case of $\alpha = 1$, instead of the time-domain technique introduced above, conventional analysis techniques, which are relatively simpler and more familiar for practical engineers, can also be used for dynamic analyses.

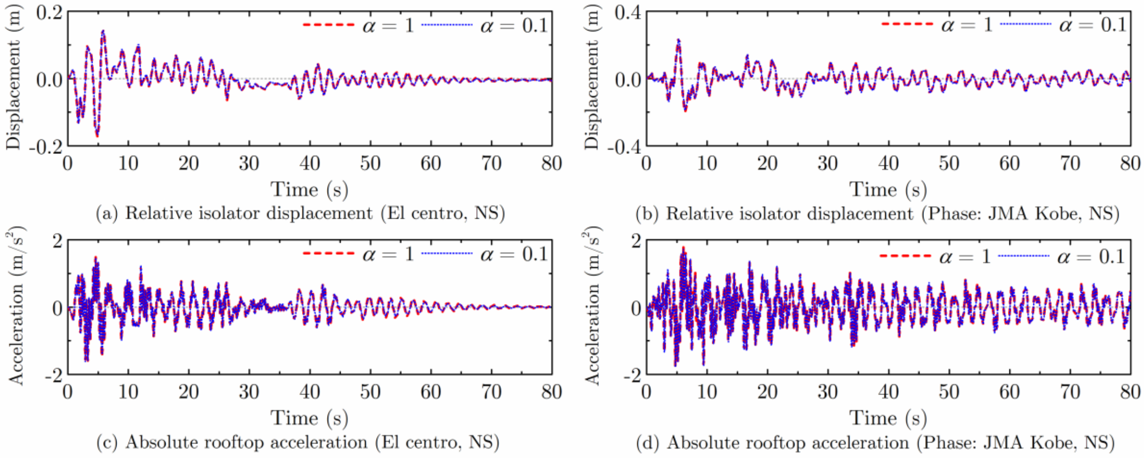

Fig. 9 – Time-history responses of a base-isolated structure incorporated with RILD (nonlinear case)

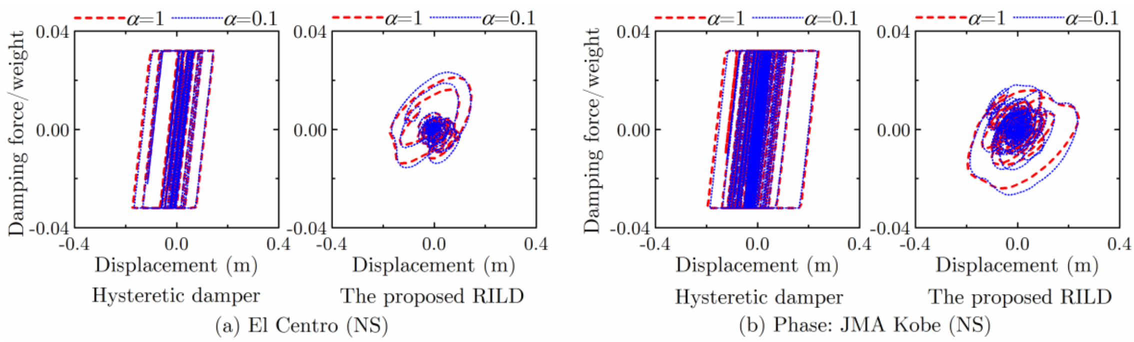

Fig. 10 – Hysteresis loops of HDs and the proposed RILD elements

4.3 Parametric studies

In the above subsections, the proposed RILD elements with $\alpha = 1$ and $\alpha = 0.1$ are considered for comparison. In order to further investigate the performance differences between the proposed RILD elements with different turning parameters α, when incorporated into a base-isolated structure, a number of nonlinear time-history analyses are conducted using the six ground motions whose acceleration spectra are shown in Fig. 6. The maximum seismic responses, in terms of the isolator displacement and the floor response acceleration, among those obtained by separately using the six ground motions, are considered as performance indices.

For example, by fixing $\eta = 0.4$ and increasing the tuning parameter α from 0.1 to 1.0 with a step size of 0.1, Fig. 11 shows the performance indices varying against the tuning parameter α, where both the linear case ($\mu = 0$) and nonlinear case ($\mu = 3.2\%$) are considered. It is shown that in both the cases, the value of α generally has a limited effect on the performance indices. It should be mentioned that in the limiting case of $\alpha = 1$, the proposed model reduces to an integer-order derivative system, which is relatively simpler to be analyzed by use of conventional dynamic analysis methods and also more familiar for practical engineers, compared to a fractional-order case. Therefore, combining with the results of parametric studies, it is suggested that in order to causally approximate the ideal non-causal RILD for application into a base-isolated structure, the Keivan model (the proposed model with $\alpha = 1$) can be used as a simple option without compromising the accuracies of both linear and nonlinear dynamic analyses.

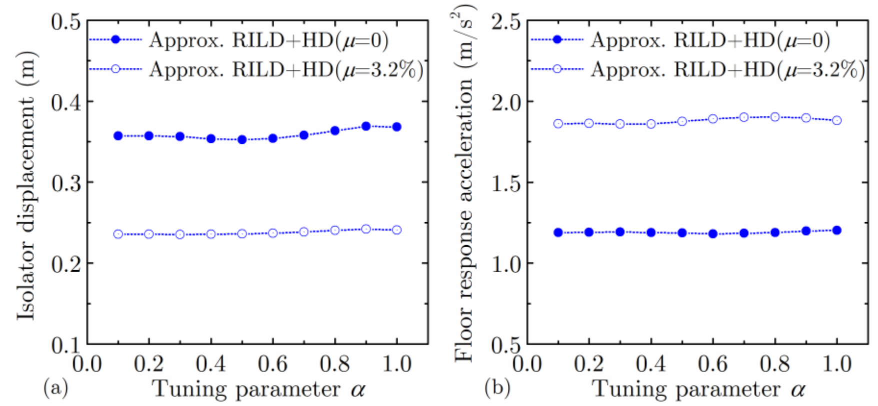

Fig. 11 – Parametric studies with respect to tuning parameter α ($\eta = 0.4$)

5. Conclusions

In this study, a generalized model is proposed to causally approximate RILD using the concept of the fractional-order derivative. It is found that with orders of zero and unity, the proposed model reduces to the Makris and the Keivan models, respectively. This means that the proposed model actually represents a continuous transformation from the Makris to the Keivan models with a tuning parameter α increased from zero to unity, i.e., it is indeed a generalized mode of causally approximated RILD. For the numerical implementation of the proposed model, a time-domain analysis technique is developed, which can be readily incorporated into the established numerical integration schemes, so that the dynamic analyses of a structural system incorporated with the proposed model can be conducted. A five-story base-isolated building structure is used as an analytical example, and both hysteretic damper and the proposed approximated RILD element are incorporated into the isolation layer for providing additional damping to constraint the isolator displacements. A number of time-history analyses are conducted to verify the effectiveness of the developed time-domain technique for nonlinear dynamic analyses. Furthermore, parametric studies are conducted to investigate the effect of the tuning parameter α on the seismic performance of the controlled structure. It is suggested that in order to causally approximate the ideal non-causal RILD for application into a base-isolated structure, Keivan model (the proposed model with $\alpha = 1$) can be used as a simple option without compromising the accuracies of dynamic analyses.

Acknowledgments

The first author is supported by a fellowship from the Japan Society for the Promotion of Science (JSPS). This work is supported by a Grant-in-Aid for Encouragement of JSPS Research Fellows (No. 19J11299).

Copyrights

References

[1] Ikago K, Inoue N (2014): Behavior of rate-independent linear damping incorporated into long-period structures subjected to strong ground motions. *Proceedings of Sixth World Conference on Structural Control and Monitoring*, Barcelona, Spain.

[2] Crandall SH (1963): Dynamic response of systems with structural damping, in: S. Lees (Ed.), *Air, Space, and Instruments, Draper Anniversary Volume*, McGraw-Hill Book Co., New York, 183-193.

[3] Biot M (1958): Linear thermodynamics and the mechanics of solids. *Proceedings of the Third US National Congress of Applied Mechanics, American Society of Mechanical Engineers*, New York, 1-18.

[4] Caughey T (1962): Vibration of dynamic systems with linear hysteretic damping (linear theory). *Proceedings of Fourth US National Congress of Applied Mechanics, American Society of Mechanical Engineerings*, New York, 87-97.

[5] Makris N (1997): Causal hysteretic element. *Journal of engineering mechanics*, **123** (11), 1209-1214.

[6] Keivan A, Phillips BM, Ikenaga M, Ikago K (2017): Causal Realization of Rate-Independent Linear Damping for the Protection of Low-Frequency Structures. *Journal of Engineering Mechanics*, **143** (9), 04017058.

[7] Keivan A, Phillips BM, Ikago K (2018): Adaptive causal realization of rate-independent linear damping. *Engineering Structures*, **167**, 256-271.

[8] Luo H, Chong C, Ikago K, Keivan A, Phillips B (2018): Passive implementation of rate-independent linear damping using a negative stiffness element. *Proceedings of the 11th National Conference in Earthquake Engineering*, Earthquake Engineering Research Institute, Los Angeles, CA.

[9] Luo H, Ikago K, Chong C, Keivan A, Phillips BM (2019): Performance of low-frequency structures incorporated with rate-independent linear damping. *Engineering Structures*, **181**, 324-335.

[10] Ikago K, Luo H, Fukuda I, Li D (2019): A first-order approximation of Biot's model to realize rate-independent linear damping. *Proceedings of the Tohoku Chapter meeting of the Architectural Institute of Japan*, Iwate, Japan.

[11] Luo H, Fukuda I, Hanzawa Y, Li D, Ikago K (2019): A causal fractional-order filter to approximate the performance of rateindependent linear damping. *Proceedings of annual meeting of the Architectural Institute of Japan*, Kanazawa, Japan, 913-916.

[12] Makris N, Constantinou M (1991): Fractional-derivative Maxwell model for viscous dampers. *Journal of Structural Engineering*, **117** (9), 2708-2724.

[13] Spanos PD, Evangelatos GI (2010): Response of a non-linear system with restoring forces governed by fractional derivatives—Time domain simulation and statistical linearization solution. *Soil Dynamics and Earthquake Engineering*, **30** (9), 811-821.

[14] Sarlis AA, Pasala DTR, Constantinou M, Reinhorn A, Nagarajaiah S, Taylor D (2012): Negative stiffness device for seismic protection of structures. *Journal of Structural Engineering*, **139** (7), 1124-1133.

[15] Luo H, Hanzawa Y, Ikago K (2018): Seismic performance enhancement of a base-isolation structure by using a passive rate-independent damping model. *Proceedings of the 7th Asia Conference on Earthquake Engineering*, Bangkok, Thailand.

[16] Samko SG, Kilbas AA, Marichev OI (1993): *Fractional integrals and derivatives (theory and applications)*. Gordon and Breach, Switzerland.

